# Three-Dimensional Structure and Position of Porcine Motilin in Sodium Dodecyl Sulfate Micelles Determined by $^1$H NMR†

Jüri Jarvet, Janusz Zdunek,‡ Peter Damberg, and Astrid Gräslund*

*Department of Biophysics, Arrhenius Laboratories, Stockholm University, S-106 91 Stockholm, Sweden*

*Received January 27, 1997*⊗

ABSTRACT: The solution structure of the porcine gastrointestinal peptide hormone motilin was determined in the presence of sodium dodecyl sulfate (SDS) micelles at 28 °C using $^1$H nuclear magnetic resonance, full relaxation matrix analysis, and structure calculations based on restrained molecular dynamics. The structure of motilin in SDS micelles is described by a reverse $\gamma$-turn and a $\beta$-turn of type II in the N terminal end, an α-helical region in the middle of the molecule, and an extended structure at the C terminus. The position of the motilin molecule relative to the SDS micelles was probed by adding spin-labeled stearic acids, containing 12-doxyl or 5-doxyl spin-labels. We observed selective broadening of the proton resonances of residues 3−5 and concluded that they must be located in the interior of the micelle. These experiments suggest a structural model in which the hydrophobic N terminus consists of two well-defined turns buried in the interior of the micelle, whereas the amphiphilic α-helical part is located at the surface of the micelle. Spectral density mapping using a $^{13}$C label on the $^{\alpha}$C of Leu$^{10}$ gave overall rotational correlation times $\tau_m$ of 6.6 and 4.5 ns at 35 and 45 °C, respectively. The long correlation time in combination with a high order parameter ($S = 0.92$) indicates that motilin has a rigid structure in the complex with the SDS micelle.

Motilin is a linear peptide hormone with 22 amino acid residues. It is found mainly in the gut where it stimulates the contractions of the gastrointestinal smooth muscle (Mutt, 1982; McIntosh & Brown, 1988). Its presence in the brain or in nerves has been debated, and any role as a neurotransmitter has not been established, although motilin has been shown to modulate the action of certain neural tissues [for a review see Poitras (1994)].

The biological effects of motilin are mediated by receptors in the gastrointestinal tract (Depoortere et al., 1993). The receptors are associated with phospholipid membranes, and a molecular mass of about 100 kDa has been suggested for the receptor (Depoortere et al., 1993). Other studies have shown that muscle receptors are coupled to a G protein for further intracellular signaling (Depoortere et al., 1990a,b). The localization of motilin receptors as well as the hormonal mode of action seems to vary among species (Poitras et al., 1996).

A number of potential clinical and biological applications have stimulated a large interest in the basic structure−function relationships for motilin. An unexpected finding was that the antibiotic erythromycin, a so-called macrolide, is a potent agonist (Peters et al., 1989; Depoortere et al., 1990a,b; Koga et al., 1994). Several lines of experiments have indicated that the N terminal residues of motilin are essential for the contractile activity of the hormone (Poitras et al., 1992; Macielag et al., 1992; Peeters et al., 1992; Miller et al., 1995). Particularly residues 1, 2, 4, and 7 are involved in receptor contact (Macielag et al., 1994). Recent work on motilin fragments, where the amide carbonyl groups were selectively reduced, has shown that the biological activity of motilin is strongly dependent on the rigidity of the amide bonds of the N terminal residues (Boulanger et al., 1995).

Porcine (and human) motilin has the sequence FVPIF TYGEL QRMQE KERNK GQ (Brown et al., 1973; Schubert & Brown, 1974). The N terminal end (1−8) is hydrophobic, whereas the C terminal end (9−22) is mainly hydrophilic, with a number of charged residues. Residues 1−6 are strongly conserved. The solution structure of motilin has been determined by NMR in an aqueous solution of 30% HPF[1] (Khan et al., 1990; Edmondson et al., 1991). For this structure, it was found that a wide turn was formed involving residues 3−6, whereas residues 9−20 formed an α-helical structure. The influence of solvents such as fluorinated alcohols on peptide structures has been studied for peptides derived from the BPTI sequence (Kemmink & Creighton, 1995) and the PhoE signal peptide (Chupin et al., 1995). For the PhoE signal peptide, it was found that the solution structure in TFE had more α-helical contributions than a structure determined in SDS micelles. In the case of four BPTI fragments, studied in a TFE-containing solvent (Kemmink & Creighton, 1995), it was shown that there is a correlation between the induced content of α-helix and the predicted helical propensities. TFE enhances intermolecular

† This work was supported by grants from the Swedish Natural Science Research Council, the Magnus Bergvall Foundation, and the Carl Trygger Foundation. A fellowship to J.J. from the Wenner-Gren Center Foundation is gratefully acknowledged.

* To whom correspondence should be addressed.

‡ Present address: Department of Medical Biochemistry and Biophysics, University of Umeå, S-901 87 Umeå, Sweden.

⊗ Abstract published in *Advance ACS Abstracts,* June 15, 1997.

[1] Abbreviations: SDS, sodium dodecyl-$d_{25}$ sulfate; HFP, 1,1,1,3,3,3-hexafluoro-2-propanol-$d_2$; TSPA, 3-(trimethylsilyl)propionic acid-*2,2,3,3-d*$_4$; TOCSY, total correlation spectroscopy; BPTI, bovine pancreatic trypsin inhibitor; MARDIGRAS, matrix analysis of relaxation for discerning the geometry of an aqueous structure; MD, molecular dynamics; SA, simulated annealing; rmsd, root mean square deviation; NOE, nuclear Overhauser enhancement; NOESY, nuclear Overhauser enhancement spectroscopy; ISPA, isolated spin pair approximation; CMC, critical micelle concentration; TFE, 2,2,2-trifluoroethanol; HPLC, high-performance liquid chromatography.

S0006-2960(97)00193-1 CCC: $14.00 

α-helix and β-hairpin formation, but not β-sheet formation (Sönnichen et al., 1992). In general, it seems that fluorinated alcohols like HFP and TFE have a tendency to stabilize preferentially an α-helical conformation.

Here, we present the three-dimensional structure of porcine motilin in a membrane-like environment, i.e. in the presence of SDS micelles. SDS is frequently used as a detergent to dissolve peptides or proteins, as it forms stable micelles with small aggregation numbers and undergoes relatively rapid reorientation in aqueous solution. Particularly the three-dimensional structure involving the hormonally essential N terminal residues is well-defined in this solvent. Using stearic acid-derived spin-labels associated with the micelles, we have also been able to probe the location of the peptide relative to the interior and surface of the micelle, a method that was previously used for other micelle-bound peptides (Brown et al., 1982; Papavoine et al., 1994; Chupin et al., 1995). Furthermore, by studies of a peptide with a specific $^{13}C$ label incorporated at the α-position of Leu$^{10}$, we have investigated the dynamics of the peptide in the micelle complex.

The results provide a comprehensive description of several of the molecular characteristics, which should be relevant for the receptor interaction of motilin. In addition, they provide an interesting insight into the interplay between the three-dimensional structure and dynamics of a peptide molecule, which is relatively flexible and unstructured in an aqueous solution. The peptide appears to become rigid as well as structured when its hydrophobic part inserts itself into the interior of the SDS micelle, while its amphiphilic helical part resides at the micelle surface.

## EXPERIMENTAL PROCEDURES

### *Materials*

Motilin was synthesized by the solid phase method and purified by HPLC (Allard et al., 1995). The NMR sample containing SDS was prepared by dissolving lyophilized motilin powder to an about 3 mM concentration in 300 mM SDS solution in $H_2O$, containing 10% $D_2O$. The pH of the sample was 3.4, from a direct uncorrected pH-meter reading.

The NMR sample containing HFP was prepared by dissolving lyophilized motilin powder to an about 6 mM concentration in 20 mM deuterated acetic acid in 600 μL of $H_2O$ with 30% (v/v) fully deuterated HFP and 10% (v/v) $D_2O$. The pH of the sample was 3.8, from a direct uncorrected pH-meter reading. The sample volume was 600 μL in the 5 mm sample tube, type 535-PP (Wilmad). Fully deuterated HFP was obtained from Sigma.

The 5-doxylstearic acid and 12-doxylstearic acid were purchased from Synvar, and methanol-$d_4$ was purchased from Merck. Deuterated SDS-$d_{25}$ (98%) was purchased from the Cambridge Isotope Laboratories.

### *NMR Spectroscopy*

All NMR spectra were recorded using a VARIAN Unity spectrometer operating at a 600 MHz proton frequency. An inverse detection triple-resonance probe was used. The spectral width in the proton dimension was 6 kHz, and proton chemical shifts were referenced to internal 3-(trimethylsilyl)-propionic acid-*2,2,3,3-d*$_4$ (TSPA). All two-dimensional spectra were recorded in a pure absorption phase mode of States et al. (1982). The number of data points reported are complex in the $t_2$ dimension and hypercomplex in the $t_1$ dimension. Spectra were processed using the FELIX program (version 2.30, Biosym Inc.) on a Silicon Graphics workstation. In all experiments, low-power water presaturation was used and the residual water signal in the spectra was removed by postacquisition time-domain convolution by a Gaussian function.

NOESY spectra (Jeener et al., 1979; Kumar et al., 1981) were recorded with mixing times of 100, 200, and 300 ms at 28 °C. Two-dimensional spectra were collected as a 512 ($t_1$) × 2048 ($t_2$) points time domain matrix with 48 scans per $t_1$ increment. Data were transformed after zero filling in both dimensions into 2048 points of frequency domain spectra.

TOCSY spectra (Bax & Davis, 1985; Griesinger et al., 1988) were recorded with a clean MLEV (Levitt et al., 1982) mixing sequence. The mixing times here include the delays of the clean-TOCSY pulse scheme of 40 μs. For the sample with SDS micelles, the spectra were run at 28 and 45 °C using mixing times of 30 and 60 ms, respectively. Two-dimensional spectra were collected as a 512 ($t_1$) × 2048 ($t_2$) points time domain matrix with 40 scans per $t_1$ increment. Data were transformed after zero filling in both dimensions into 2048 points of frequency domain spectra. A squared sine bell window function with 3 Hz exponential line broadening was applied.

DQF-COSY spectra of motilin in SDS and HFP-containing solvents were run with similar parameters at 28 °C. The $^3J_{H^\alpha H^N}$ spin−spin coupling constants were determined from extracted one-dimensional slices in the $\omega_2$ dimension through each resolved antiphase cross-peak in the DQF-COSY spectra. Two-dimensional spectra were collected as 512 ($t_1$) × 2048 ($t_2$) points time domain matrices with 40 scans per $t_1$ increment. Data were transformed after zero filling in the $\omega_2$ dimension into 8192 points of frequency domain spectra. The final digital resolution was 0.75 Hz/point in the $\omega_2$ dimension. A double Lorentzian antiphase model line shape, taking into account the baseline offset and slope, was fitted to each extracted one-dimensional slice.

The dynamics of motilin associated with the SDS micelle were characterized using the spectral density mapping technique (Peng & Wagner, 1992; Allard et al., 1995). The sample was motilin with a specific $^{13}C$ label at $C^\alpha$ of Leu$^{10}$. Six dipolar relaxation rates of the Leu$^{10}$ $^1H^\alpha-^{13}C^\alpha$ spin system were measured using sensitivity-enhanced inverse detected pulse sequences (Dayie & Wagner, 1994).

*Spin-Label Experiments*. The samples used in the spin-label experiments were prepared by dissolving lyophilized motilin powder to an about 1−2 mM concentration in 300 mM SDS-$d_{25}$ in 600 μL of 90% $H_2O$/10% $D_2O$. The pH was adjusted to 3.3 with HCl. The 5-doxylstearic acid and 12-doxylstearic acid were solubilized in methanol-$d_4$, to obtain 0.3 M stock solutions which were added to the samples to about 2−5 mM concentrations. This corresponds to approximately 0.5−1 spin-label per micelle, assuming about 60 SDS molecules per micelle (Israelachvili, 1991).

The position of the spin-label relative to the SDS chain in the micelle was determined using directly detected $^{13}C$ NMR, with proton decoupling on the samples containing protonated SDS and spin-labeled stearic acids or deuterium decoupling of the samples containing SDS-$d_{25}$ with spin-labeled stearic acids and peptide.

*Structure Calculations*

*Generation of Starting Structures*. Structure calculations were performed on a Silicon Graphics workstation. Ten structures of motilin were used as initial conformations in the program MARDIGRAS which performs relaxation matrix calculations to generate distance constraints (Borgias & James, 1990). The program MARDIGRAS was kindly provided by T. L. James (University of California, San Francisco). The initial structures were chosen from the trajectory of a previously performed free molecular dynamics simulation of motilin in water (J. Zdunek, L. Nilsson, and A. Gräslund, to be published) with the requirement that they represent quite different conformations. The ten structures had a rmsd not smaller than 5 Å in pairwise comparisons. The advantage of choosing the model structures of motilin from molecular dynamics calculations relies on their energetically favorable and locally correct covalent geometries.

*Determination of Distance Constraints*. A 100 ms two-dimensional NOESY spectrum was used to extract the experimental intensities for the cross-peaks of the involved protons. Distance constraints were evaluated from the experimental intensities using the complete relaxation matrix algorithm program MARDIGRAS to take into account the effects of spin diffusion. NOESY spectra with 200 and 300 ms mixing times were not used in structure calculations, but only for assignment purposes. Intensities were measured as a mean of the upper and lower parts of the two-dimensional NOESY spectrum if the difference of their intensities was less than 2-fold. When the two intensities differed by more than 2-fold, due to the residual water signal or ridges from sharp lines in the spectrum, the intensity of the line from the flat baseline part of the two-dimensional spectrum was used. Totally, we were able to extract 245 intensities from the spectrum. These intensities together with the ten model structures of motilin obtained from the previously performed MD simulation were used as input information to MARDIGRAS to calculate the distance constraints. A total number of 216 distances, 125 intraresidual and 91 interresidual, was generated by MARDIGRAS. The remaining 29 distances were found not to be essential for structure determination. From the ten sets of distances (and ranges), we used the extremes of the ranges as final lower and upper bounds of distance constraints applied in the further refinement procedure. The average difference between the upper and lower bounds, as calculated by MARDIGRAS, was 0.589 Å. In several cases, mostly involving methyl or methylene groups, the derived ranges were too restrictive. In such cases, doing some preliminary simulated annealing calculations, we were able to estimate the necessary corrections as outlined in Cooke et al. (1992). The functional form of the $V_{NOE}$ term used in primary simulated annealing was of the type "SOFTsquare", while the $V_{NOE}$ used in the refinement was of the type "SQUAre-well". Both potentials are described in detail in the manual for the program X-PLOR version 3.0 (Brünger, 1992).

*Generation of Torsion Angle Constraints*. The constraints on Φ backbone torsion angles determined from experimentally obtained $H^N-H^\alpha$ coupling constants provided additional geometric information. The torsion angles were calculated using the relationship between the Φ angle and the $^3J_{H^\alpha H^N}$ coupling constant given by the Karplus equation (Sutcliffe, 1993):

$$^3J_{H\alpha HN} = 6.4\cos^2(\Phi-60) - 1.4\cos(\Phi-60) + 1.9 \quad (1)$$

The Φ torsion angle in the polypeptide backbone is defined by the C($i-1$)−N($i$)−CA($i$)−C($i$) atoms with a Φ of 180° for the extended conformation. The calculated torsion angles were then used as parameters in the $V_{CDIH}$ energy term in the potential. The functional form of the $V_{CDIH}$ is described by

$$V_{CDIH} = S\sum C\ \text{well}[\text{modulo}_{2\pi}(\Phi-\Phi_0),\Delta\Phi]^2 \quad (2)$$

where the sum is the overall constrained torsion angles, and the well($a$,$b$) is given by

$$\text{well}(a,b) = \begin{cases} a-b & \text{if } a > b \\ 0 & \text{if } -b < a < b \\ a+b & \text{if } a < -b \end{cases} \quad (3)$$

where $S$ is the weighting factor, $C$ is the force constant, $\Phi_0$ is the torsion angle, and $\Delta\Phi$ is the range (Brünger, 1992).

*Molecular Dynamics Protocol*. Three of the most divergent structures of motilin chosen from the previously described ten structures obtained from an MD simulation of motilin in water were applied as starting conformations in new simulated annealing MD calculations using the program X-PLOR (Brünger, 1992). The potential used in the calculation was as given below:

$$V = V_{bond} + V_{angle} + V_{improper} + V_{repel} + V_{NOE} + V_{CDIH} \quad (4)$$

The first three terms describe the covalent potential as commonly used in most MD programs with the exception of using $V_{improper}$ for both planar and chiral groups of atoms. The last two terms represent the potential used for distance constraints ($V_{NOE}$) and for torsion angle constraints ($V_{CDIH}$). The remaining term ($V_{repel}$) acts as a van der Waals repulsive term and is essential for the type of calculations performed here. The functional form of this term is given by Nilges et al. (1988):

$$V_{repel} = \begin{cases} 0 & \text{if } r \geq (sr_{min}) \\ k_r(s^2 r_{min}^2 - r^2)^2 & \text{if } r < (sr_{min}) \end{cases} \quad (5)$$

where $r_{min}$ is the standard value of the van der Waals radius in the Lennard-Jones potential, $s$ is a scaling factor, and $k_r$ represents the repulsion constant. The setting of $k_r$ to a low value results in a "path through" effect for the involved atoms needed in some instances of molecular dynamics, whereas increasing the $k_r$ value prevents inconvenient close contacts between the atoms (Nilges et al., 1988).

The force constants for the covalent potential terms were set to 1000 kcal mol$^{-1}$ Å$^{-2}$, 500 kcal mol$^{-1}$ rad$^{-2}$, and 500 kcal mol$^{-1}$ rad$^{-2}$ for $k_{bond}$, $k_{angle}$, and $k_{improper}$, respectively. The SA protocol was applied as in Brünger (1992) with some modifications of the length of the high-temperature period and the cooling period. They were set to 12 000 and 6000 steps, respectively. The search of the conformational space was speeded by scaling up the masses of all the atoms by 100 because this, in turn, gave the possibility of using a long integration step of 5 fs which speeded the dynamics. The initial temperature was set to 1000 K. During the initial minimization, 100 steps of the Powell minimization algorithm were performed before entering into the dynamics, and

the force constant $V_{repel}$ was reduced by a factor 0.002. The $k_{NOE}$, with an asymptote multiplied by 0.1, was set to 50 kcal mol$^{-1}$ Å$^{-2}$, while the $k_{CDIH}$ was kept at 5 kcal mol$^{-1}$ rad$^{-2}$. The first part of the high-temperature dynamics consisted of 8000 steps (40 ps) with coupling to the temperature bath at 1000 K. Additionally, for this period of simulations, the weights of $V_{angle}$ and $V_{improper}$ were decreased by factors 0.4 and 0.1, respectively. During the second period of the high-temperature dynamics (20 ps), the force constants for all covalent terms and the scaling of the asymptote of $V_{NOE}$ were reset to their initial values. The succeeding cooling period consisted of 6000 steps divided in 18 cycles as going from 1000 K to the final temperature of 1000 K. The force constant $k_{CDIH}$ was kept here at 200 kcal mol$^{-1}$ rad$^{-2}$. During the cooling period, the $k_r$ was gradually increased every cycle from an initial value of 0.003 to a final value of 4 kcal mol$^{-1}$ Å$^{-2}$, which was found to be sufficient to ensure that no close nonbonded contacts occur (Brünger, 1992). In concert with increasing the $k_r$, the scaling parameter *s* in eq 5 was gradually decreased from 0.9 to the final 0.75, resulting in the hard sphere radii of 0.75 of their Lennard-Jones values [a value commonly applied in distance geometry programs (Brünger, 1992)]. All SA calculations were followed by 500 steps of Powell minimization.

Further refinement of structures was performed using an additional SA protocol consisting of the cooling period (8000 steps, 40 ps) from 1000 to 100 K and also followed by energy minimization as before. Starting from every initial structure of motilin, we generated 40 refined structures. In total, 120 structrues were created for motilin in the SDS micelle environment.

## RESULTS

### *NMR Spectroscopy*

NMR structure studies were performed on a sample of 3 mM motilin in 300 mM SDS. The choice of SDS concentration is critical for the high-resolution spectra. The number of SDS molecules forming a micelle is around 60 (Israelachvili, 1991). For a 300 mM SDS concentration, it follows that the molar concentration of micelles is about 5 mM. For a peptide concentration of less than 5 mM, one is most likely to find not more than one motilin molecule per SDS micelle. In NMR structure studies, a high SDS concentration, substantially higher than the critical micelle-forming concentration, and giving a solute/micelle ratio well below unity, was earlier found to improve the quality of NMR spectra (McDonnell & Opella, 1993). However, with increasing SDS concentrations, the solution becomes more viscous (Chari et al., 1993), which results in longer correlation times and broader resonances. At very high concentrations, SDS forms rod-shaped aggregates rather than spherical micelles (Israelachvili, 1991).

*Assignment*. For the structure determination of porcine motilin in the SDS environment, the distance constraints used were measured from the 100 ms mixing time NOESY spectrum and Φ dihedral constraints from DQF-COSY experiments at 28 °C. The proton resonance assignment procedure was started using TOCSY spectra of motilin in 300 mM deuterated SDS in $H_2O$, recorded at 28 and 45 °C. At the higher temperature used, all the cross-peaks in the TOCSY fingerprint region are present (Figure 1), whereas

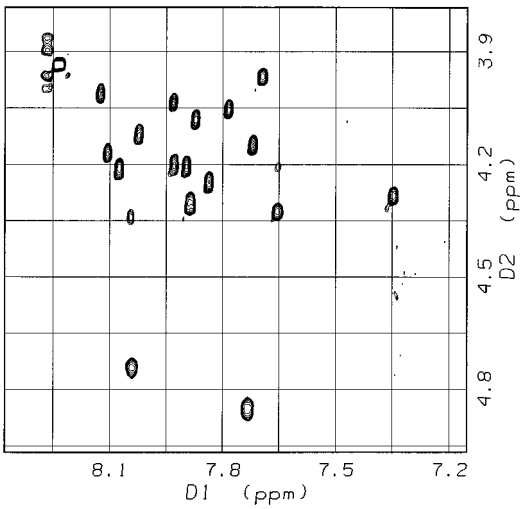


FIGURE 1: TOCSY fingerprint region of motilin in 300 mM SDS at 45 °C. The spectrum was recorded with a 60 ms mixing time at 600 MHz.

at 28 °C, the Asn[19] cross-peak at 4.62 ppm is missing due to overlap with the water presaturation frequency. Proton resonance assignment was done using standard methods. The assignment was started by observing that there were two cross-peaks with the same NH frequency (7.66 ppm) in the fingerprint region of the TOCSY spectrum (Figure 1). This NH was assigned to Thr[6]. The sequential assignment was straightforward from Phe[5] to Gln[22] using $NH_i-NH_{i+1}$ connectivities in the 300 ms NOESY spectrum as shown in Figure 2A.

Figure 2B shows the fingerprint region of the same NOESY spectrum with some assignments indicated and $\alpha H_i-NH_{i+1}$ connectivities shown. There are a number of overlapping cross-peaks in this region, since there are a number of residues with identical chemical shifts of both αH and NH resonances. A number of important constraints for the helical part of the sequence overlap, which make the α-helix appear more ill-defined than it may be in reality. Figure 2C shows long-range connectivities found between γ-protons of Leu[10] and aromatic protons of Phe[5] and Tyr[7]. The boxed region in Figure 2C contains e.g. a cross-peak at 7.2 and 0.91 ppm between the Leu[10] γ-proton and the 3,5-protons of Phe[5]. This is a unique rather long-range connectivity which is a first indication of a relatively well-defined solution structure in this part of the molecule. The long-range connectivities (Figure 2C, boxed region) help to connect the two parts of the molecule, the hydrophobic N terminus and the more hydrophilic C terminus, with each other.

Figure 3 shows the number of NOE cross-peaks, inter- and intraresidual, which are related to each residue along the sequence. The average number of constraints for residues 2−7 is quite high (22 per residue), which is another indication that it may be possible to determine the structure in this particular region quite accurately. The proton chemical shifts and overlapping chemical shifts and the $^3J_{H^\alpha H^N}$ spin−spin coupling constants are given as Supporting Information. Corresponding NMR spectra were also recorded in 30% HFP solvent at 21 °C (data not shown), and the obtained $^3J_{H^\alpha H^N}$ values are included as Supporting Information.

*Secondary Chemical Shifts*. As a first step in the structure determination, the secondary chemical shifts of the α-protons

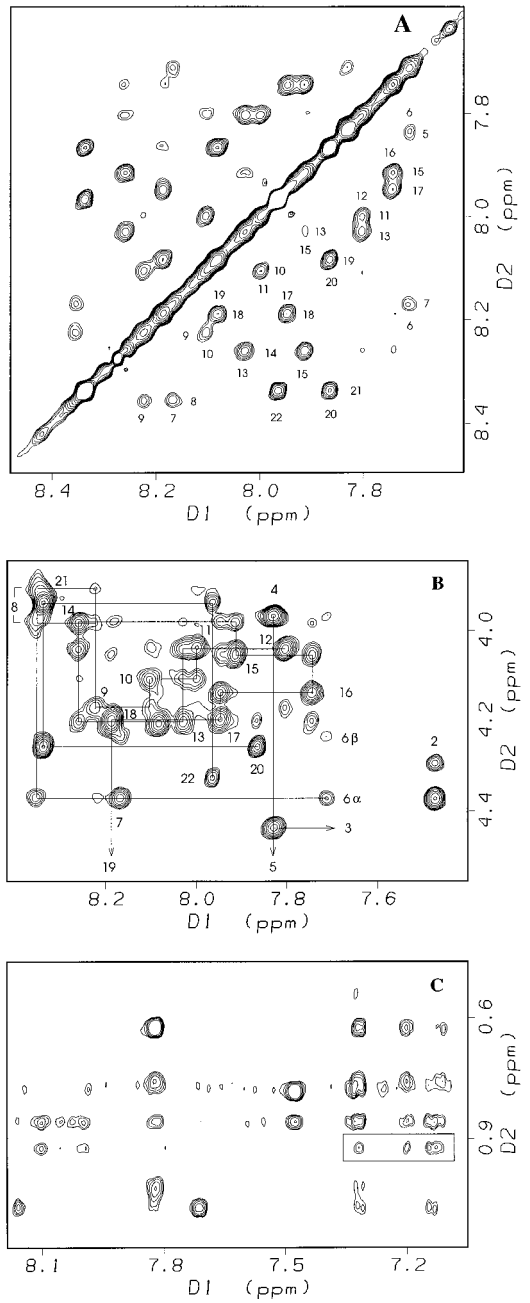


FIGURE 2: Regions of a 300 ms mixing time NOESY spectrum of motilin in 300 mM SDS at 28 °C recorded at 600 MHz. (A) In the NH−NH region, sequential connectivities are indicated by amino acid residue numbers. (B) In the fingerprint NH−αH region, residues 5 and 19 are not included. (C) In the NH−$\gamma$H region, the region of long-range connectivities between residues 5 and 10 is indicated by a box.

were calculated as a difference between random coil chemical shifts (Wüthrich, 1986) and experimentally observed shifts. In order to minimize local fluctuations, a mean secondary shift over three residues was calculated (Arvidsson et al., 1994). In Figure 4, the secondary chemical shifts of the α-protons of motilin are compared in 30% HFP at 21 °C [cf. Khan et al., (1990)] and in SDS at 28 and 45 °C. For the helical part of the molecule, from residue 9 to 20, the secondary chemical shifts are very similar in the two solvents. For both termini, the secondary chemical shifts in the presence of SDS indicate higher structure content at the lower temperature. For the N terminal end, the secondary chemical shifts are clearly different, particularly when comparing the

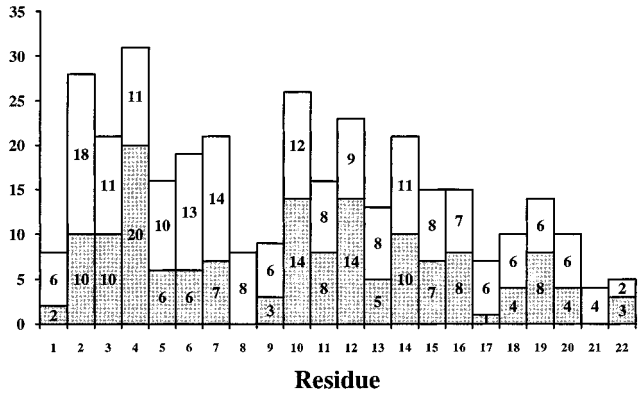


FIGURE 3: Number of inter- (white box) and intraresidual (gray box) NOE constraints determined from 100 ms NOESY spectra for each residue of motilin in 300 mM SDS at 28 °C.

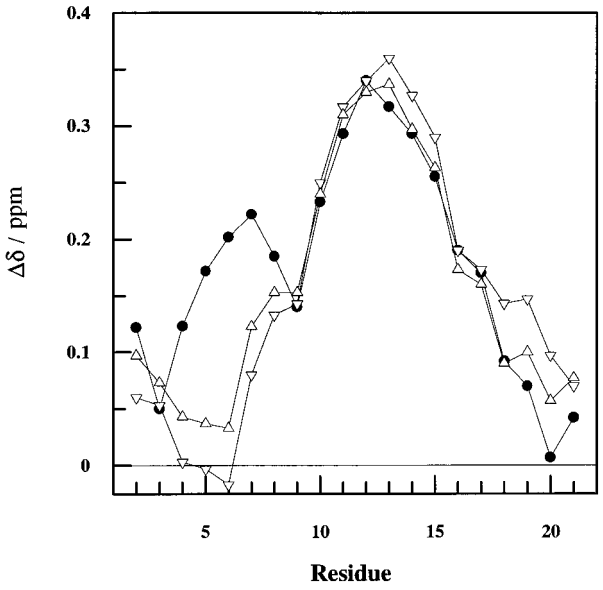


FIGURE 4: Secondary chemical shifts of $H^{\alpha}$ resonances of motilin in 30% HFP at 21 °C (●), in 300 mM SDS at 28 °C (▽), and in 300 mM SDS at 45 °C (△). The secondary shifts have been calculated relative to the random coil values (Wüthrich, 1986). All chemical shifts have been averaged over three residues, in order to suppress local fluctuations. Chemical shifts are referenced against internal TSPA.

two solvents, but also to some extent in the SDS solvent at the two temperatures.

### *Structure Calculations*

*Generation of Distance Constraints*. The ten model structures of motilin obtained from a previous MD simulation (J. Zdunek, L. Nilsson, and A. Gräslund, to be published) together with the experimental intensities extracted from two-dimensional NOESY spectra recorded with a 100 ms mixing time were used as input information to derive distance constraints using the MARDIGRAS program. The NMR *R*-factor is a measure the differences between the experimental NOESY cross-peak intensities and those predicted from a particular three-dimensional structure (Baleja et al., 1990; Nikonowicz et al., 1990). The *R*-factor for different overall rotational correlation times, calculated using MARDIGRAS, shows a minimum around 5 ns (data not shown). A mixing time of 100 ms and a single rotational correlation time of 5 ns were used in all calculations carried out by

MARDIGRAS. As the MARDIGRAS program is based on the Complete Relaxation Matrix Algorithm (CORMA) (Borgias & James, 1990), the calculated distances are more accurate than those from calculations using an ISPA method.

The MARDIGRAS-generated distances, calculated from the ten model structures of motilin, were not significantly different, indicating the ability of the program to produce an output relatively independent of the initial conformation. To ensure that the choice of ten MD-derived starting structures does not lead to biased results, we used MARDIGRAS to generate a new set of distance constraints from some additional starting structures, including random coil, extended, α-helix, and $\beta$-strand model structures. The distances generated from this secondary set of starting structures correlated well with the ones obtained from the MD structures with a correlation coefficient of 0.97 (data not shown). In order to incorporate all information obtained from the ten sets of calculated distances and ranges to the new MD simulations, we applied the extremes of the calculated ranges as upper and lower limits of the particular distance constraint. The upper and lower limits were then used as parameters in the $V_{NOE}$ energy term in the applied potential.

*Determination of Torsion Angle Constraints*. The information included in experimentally derived $H^N-H^\alpha$ coupling constants was used in determination of the Φ backbone torsion angle constraints. The torsion angle constraints together with the calculated distance constraints and the covalent potential were applied to determine the conformational space available. The Φ torsion angles are related to corresponding $^3J_{H^\alpha H^N}$ via eq 1. The 16 Φ torsion angles used in all subsequent MD calculations are included as Supporting Information. We observed that the coupling constants were larger than expected for the α-helical part of the sequence. This may be due to high uncertainty in the experimentally determined coupling constants caused by increased line widths or may indicate that the helix is rather far from an ideal α-helix. Residues with resonances either overlapping or buried under water are not included. The ambiguity of assignment of different torsion angles corresponding to the same value of a given $^3J_{H^\alpha H^N}$ coupling constant can be partially resolved by utilizing the information from the analysis of the values of the Φ angles calculated from a number of known protein structures. The values for the Φ angle obtained from such an analysis appear to be concentrated in the range of −30 to −180° (Richardson, 1981). Furthermore, a preliminary calculation of structure determination using both the distance constraints and the torsion angle constraints can be helpful in selecting the appropriate value of the Φ angles that satisfy the correct local geometry of the involved residues. The functional form of the $V_{CDIH}$ restraining term was as in eqs 3 and 4. Taking into consideration the imprecision of the experimentally derived coupling constants and hence the errors in the calculated angle centroids $\Phi_0$, we assumed the angle ranges $\Delta\Phi$ to be 30° for all values of Φ.

*Convergence of Derived Structures*. A total of 120 structures of motilin in 300 mM SDS were calculated using simulated annealing MD calculations. Of these calculated structures, 65 passed an acceptance test for ranges of bonds, angles, distance constraints, and dihedral constraints. The criteria used for the acceptance were as given below:

rmsd for bonds $<0.01$ Å

rmsd for angles $<1°$

no NOE *distance* violations $>0.5$ Å

no dihedral *angle* violations $>5°$

which are typical for very good NMR structures (Brünger, 1992). For the 55 structures that were not accepted, there were between one and four NOE violations of $>0.5$ Å (largest, 1.1 Å; average, 0.6 Å) and between zero and one dihedral angle violation of $>5°$ (largest, 19°). The variation of total energy and NOE constraint energy for the total 120 structures is shown as Supporting Information.

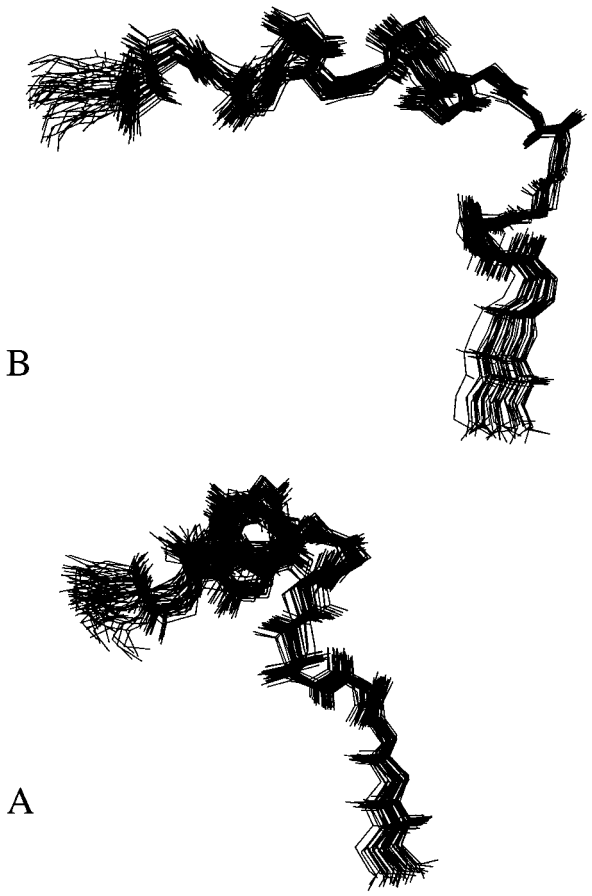


FIGURE 5: Two views of the backbone of the final structures of motilin. Forty-two structures superimposed on the structure with the lowest violations of distance constraints. rmsd < 1.23 Å between all structures.

Among the 65 accepted structures, 42 show a pairwise rmsd smaller than 1.23 Å with the structure showing the smallest violation of distance constraints (lowest $V_{NOE}$ term and also the lowest total energy). As all the accepted structures passed the tight covalent criteria stated above, we found these comparisons to be most indicative in searching for a final conformation of motilin that satisfies the imposed experimental constraints. The rmsd comparisons included all heavy atoms of the backbone of motilin and were performed for the whole sequence of the molecule, residues 1−22. Figure 5 shows two views of the backbone heavy atoms of the 42 selected structures superimposed on the conformation with the lowest energy. The other accepted structures also belong to the same conformational family and

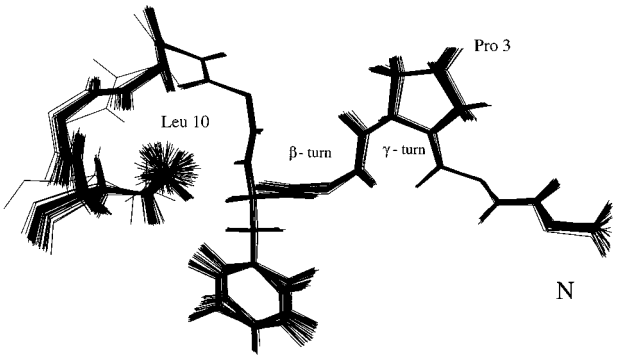


FIGURE 6: Detailed picture of the hydrophobic N terminal part of motilin (residues 1−10). Residue Pro[3] is in the cis conformation and involved in a reverse $\gamma$-turn. A $\beta$-turn of type II extends over residues Pro[3]-Ile[4]-Phe[5]-Thr[6]. A large turn creates a pocket for the side chain of residue Leu[10].

are similar. The figure shows the overall bent structure of the peptide with the α-helix present between residues 10 and 16 in the central part of the sequence. The part between residues 3 and 10 appears to have a well-defined structure. Both N and C termini have extended conformations.

Figure 6 shows a comparison where the backbone and some side chain atoms from residue Phe[1] to Leu[10] are included. The structures show an excellent agreement when we overlaid 50 of the 65 structures that have the smallest rmsd with the conformation with the lowest energy. The figure shows the presence of two well-defined turns close to the N terminus. The side chain atoms of Leu[10] are buried in the large pocket created by the main chain atoms between Phe[5] and Leu[10].

*Spin-Label Studies*. To determine the position of the motilin molecule in the micelle, the spin-labels 12-doxylstearic acid and 5-doxylstearic acid were used to produce selective broadening of the proton resonances from amino acid residues close to the spin-label. The doxyl group containing the nitroxide free radical is bound to the carbon at position 12 or 5 of the stearic acid, respectively. The positions of the spin-labels in the micelles were determined by comparing the line widths in $^{13}$C spectra of SDS in the absence and in the presence of the spin-label as outlined in Papavoine et al. (1994). It was found that 5-doxylstearic acid particularly broadens the resonances from SDS carbons 1−3 close to the micelle surface, in agreement with data in Papavoine et al. (1994). In addition, we found that 12-doxylstearic acid particularly broadens the $^{13}$C resonances from SDS carbons 10−12 close to the center of the micelle (data not shown). These experiments were performed using protonated as well as deuterated SDS in the presence and absence of motilin, with very similar results.

The effects of the spin-labels on the peptide in the micelle were measured by comparing the intensities of the TOCSY cross-peaks in the absence and in the presence of the spin-labels (Figure 7). After addition of 12-doxylstearic acid, in a spin-label to SDS ratio corresponding to about 1 spin-label per micelle, four major changes occurred in the fingerprint region of the spectra (see Figure 7A,B). The cross-peaks from residues Ile[4] and Phe[5] disappeared, while the cross-peaks from residues Val[2] and Gln[22] changed their chemical shifts. In the α,$\beta$-cross-peak region of the spectra, analogous changes were observed. The cross-peaks from residues Pro[3] and Phe[5] disappeared, and residue Ile[4] gave rise to weaker signals (data not shown).

After addition of 5-doxylstearic acid in the same spin-label to SDS ratio as that for the 12-doxylstearic acid, we made the surprising observation that the same residues (Pro[3]-Ile[4]-Phe[5]) were affected as those observed with 12-doxylstearic acid (data not shown). After further addition of 5-doxylstearic acid, to a spin-label to SDS ratio corresponding to about 3 spin-labels per micelle, most of the cross-peaks from the first seven N terminal residues were missing or reduced. In the C terminal hydrophilic part of the peptide, the cross-peaks from residues Glu[9], Leu[10], Met[13], Gln[14], Glu[17], and Arg[18] showed a decreased intensity, while cross-peaks from Gln[11], Arg[12], Glu[15], Lys[16], and Lys[20] remained comparatively intense (Figure 7C). We also observed that both $H^N$ and $H^\alpha$ of the C terminal residue Gln[22] changed their chemical shifts after addition of either spin-label. Figure 8 shows a ribbon representation of the peptide backbone, where the influence of the 5-doxyl spin-label in high concentrations is shown.

*Dipolar Relaxation Rates*. A motilin sample specifically $^{13}$C-labeled at $C^\alpha$ of Leu[10] was used to determine the dynamics of motilin in SDS. The dipolar relaxation rates of the Leu[10] $^1H^\alpha-^{13}C^\alpha$ spin system were measured at 35 °C (Figure 9A inset) and at 45 °C (data not shown), and spectral density mapping (Peng & Wagner, 1992) was carried out. The model free spectral density function (Lipari & Szabo, 1982a,b) was fitted to the experimental spectral density values at different frequencies (0, 150, 450, and 750 MHz) (Figure 9A). The dynamics of the $^1H^\alpha-^{13}C^\alpha$ vector of Leu[10] have previously been studied by spectral density mapping at three different field strengths in 30% HFP and water environments (Jarvet et al., 1996). The overall rotational correlation times $\tau_m$, the general order parameters $S^2$, and the internal correlation times $\tau_e$ describing the dynamics of this vector at 35 °C in $H_2O$, 30% HFP, and 300 mM SDS are shown in Table 1. The corresponding spectral density functions are shown in Figure 9A. The spectral density values at the proton resonance frequency are generally not well-determined (Jarvet et al., 1996) and are not included in the figure or in the model fitting.

## DISCUSSION

*Overall Structure*. All 65 accepted structures constitute the same conformation in principle with only small local differences. In the refined structure of porcine motilin in 300 mM SDS at 28 °C (Figures 5, 6, and 8), residues Phe[1] and Val[2], near the N terminus, are in an almost extended conformation. The whole hydrophobic part of motilin, residues 1−9, makes an almost right angle against the axis of the clearly observable helical part of the molecule. We observed also the last few C terminal residues protruding from the plane defined by the hydrophobic part and the axis of the helix.

The first (smaller) turn is observable at residue Pro[3] (Figure 6). This turn appears to be the result of the cis conformation of the residue Pro[3]. Pro[3] is also considered as the first residue included in the larger turn expanded also over the sequence Ile[4]−Phe[5]−Thr[6]. Another arched portion of the main chain extending over residues Thr[6]−Leu[10] creates a pocket for the two methyl groups of the side chain of Leu[10]. The apparent closer contact of the side chains of residues Leu[10] and Phe[5] is also reflected by the NOE intensities (and distance constraints) observable for the involved residues (Figure 2C).

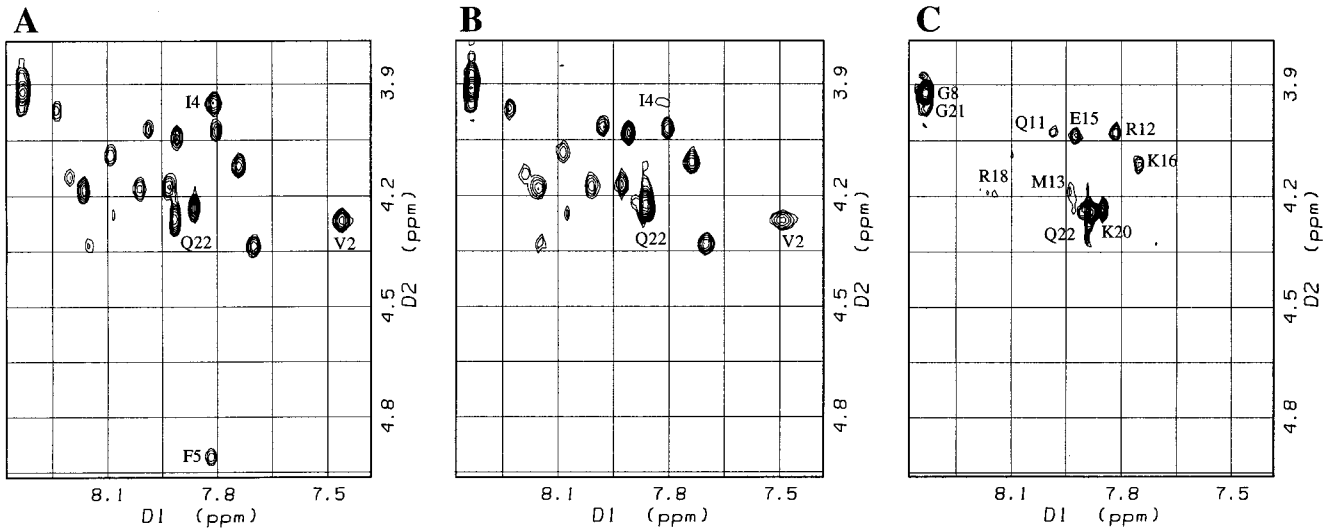


FIGURE 7: Fingerprint region of 600 MHz TOCSY spectra of motilin in 300 mM SDS at 28 °C without spin-label (A), in the presence of 5 mM 12-doxylstearic acid (B), and in the presence of 10 mM 5-doxylstearic acid (C).

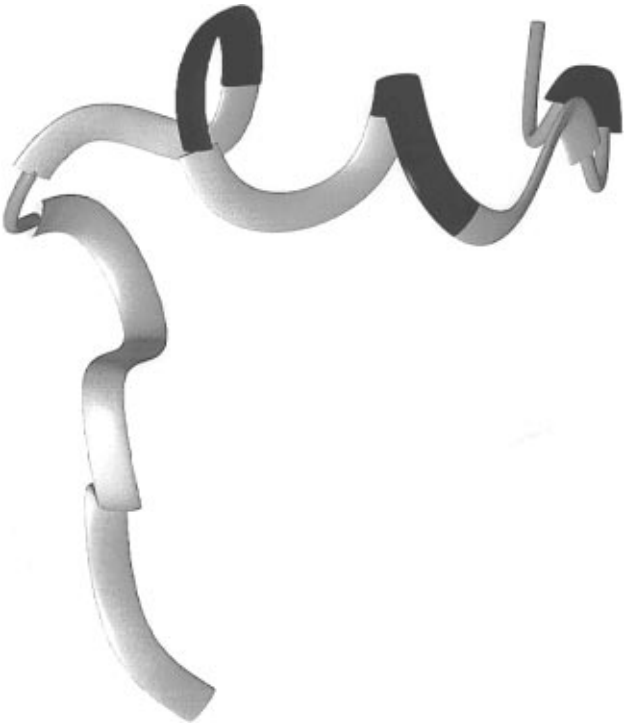

FIGURE 8: Ribbon representation of the backbone of motilin in SDS micelles. The effect of the high concentration of 5-doxylstearic acid is color-coded. Residues where the cross-peaks in the TOCSY spectra showed a decreased intensity are colored white, while residues where the cross-peaks remained comparatively intense are colored black. The following residues are shown in rounded ribbon representation: $Gly^8$ and $Gly^{21}$ have overlapping resonances, $Asn^{19}$ has its $H^\alpha$ overlapping with water, and $Gln^{22}$ has changed its chemical shifts. We conclude that the black part is outside the micelle and the white part is located in the interior of or in contact with the micelle. This figure was prepared by the program MOLMOL (Koradi et al., 1996).

On the basis of this analysis, the structure of motilin in SDS micelles may be described by $\gamma$- and $\beta$-turns at the N terminal end, an α-helical region in the middle of the molecule (residues 10−16), and an extended structure at the C terminus. It should be pointed out that these structural features are in good agreement with the secondary chemical shifts presented in Figure 4. Regions with $\beta$-structure should have a downfield shift, as observed around residue 5, and regions with α-helix structure should have a fairly large upfield shift (Pastore & Saudek, 1990), as observed for residues 10−16. Comparing the previously determined structure of motilin in 30% HFP and the present one in SDS micelles, we observe that the α-helical contribution is considerably smaller in SDS micelles. However, the N terminal turns of motilin in SDS are very well-defined at 28 °C. This result is consistent with the large number of NOE constraints involving residues 2−7 (Figure 3).

*Geometry of Turns*. Torsion angles were evaluated for the lowest-energy structure of motilin in SDS micelles at 28 °C (Supporting Information). Some of the angles will be discussed here in order to give a more precise description of the secondary structures present. The smaller turn present in the vicinity of residue $Pro^3$ is recognized as the inverse of a classical $\gamma$-turn (Creighton, 1993). $\Phi_{i+1}$ and $\Psi_{i+1}$ describe the geometry of an inverse $\gamma$-turn (Neuhaus & Williamson, 1989). Translating these indices to the numbering of amino acids, we found $\Phi_{i+1}$ corresponding to $\Phi$ of $Pro^3$ and $\Psi_{i+1}$ to $\Psi$ of $Pro^3$. For $Pro^3$, we found $\Phi = -73°$ and $\Psi = 53°$, which are close to the ideal values for the inverse $\gamma$-turn: $-70$ to $-85°$ for the $\Phi$ angle and $60-70°$ for the $\Psi$ angle. The discrepancy often found between the values observed in proteins and in the ideal geometry of reverse turns originates probably from the fact that initially the restriction on the flexibility of the peptide backbone was overestimated (Neuhaus & Williamson, 1989). Moreover, the short distance (1.89 Å) between the O of $Val^2$ and the HN of $Ile^4$ indicates that a hydrogen bond is stabilizing the inverse $\gamma$-turn (Figure 6).

The adjacent larger turn existing over residues $Pro^3-Thr^6$ shows parameters (although somewhat distorted) of the $\beta$-turn of type I (Neuhaus & Williamson, 1989). Such a turn is defined in Neuhaus and Williamson (1989) by $\Phi_{i+1}$ ($-60°$), $\Psi_{i+1}$ ($-30°$), $\Phi_{i+2}$ ($-90°$) and $\Psi_{i+2}$ (0°) to be compared with the corresponding values calculated here for $\Phi$ of $Ile^4$ ($-89°$), $\Psi$ of $Ile^4$ ($-32°$), $\Phi$ of $Phe^5$ ($-107°$), and $\Psi$ of $Phe^5$ (47°). The present turn is somewhat wider than the classical one with a O $Pro^3$−HN $Thr^6$ distance of about 3.35 Å, but as considered in Neuhaus and Williamson (1989), the hydrogen bond between residues $i$ and $i + 3$ in the $\beta$-turn is often missing (Figure 6).

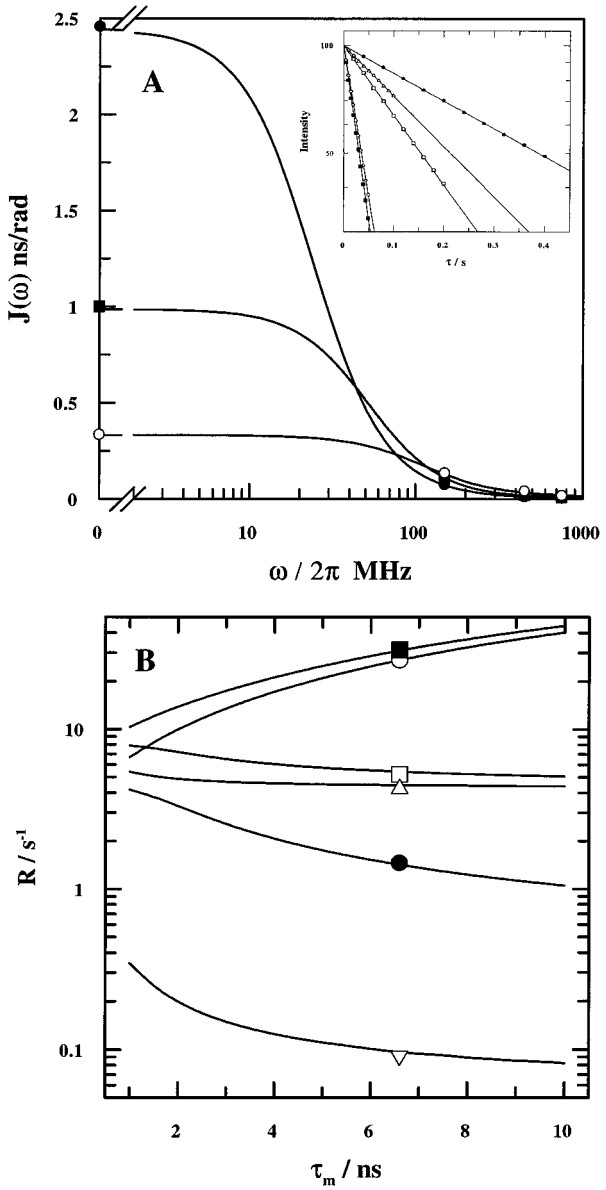


FIGURE 9: (A) Experimental spectral density values and the best-fitting model free spectral density functions at 35 °C for the $^{13}C^{\alpha}-H^{\alpha}$ vector in Leu[10] of motilin in 300 mM SDS (●), in 30% HFP (■), and in $D_2O$ (○). The relaxation rates were measured at a 600 MHz proton frequency. The parameters of the model free spectral density curves are listed in Table 1. $J(\omega_H)$ is not shown. The inset shows relaxation decays of five relaxation experiments at 35 °C for the $^{13}C-H^{\alpha}$ vector in Leu[10] of motilin in 300 mM SDS: (■) the antiphase coherence decay, with a rate $R_{CH}(2H_zC_x)$ of 22.4 $s^{-1}$; (○) the carbon in-phase transverse relaxation decay, with a rate $R_c(C_x)$ of 19.4 $s^{-1}$; (□) the longitudinal two-spin order relaxation decay, with a rate $R_{CH}(2H_zC_z)$ of 4.50 $s^{-1}$; (△) the proton longitudinal relaxation decay, with a rate $R_H(H_z)$ of 3.26 $s^{-1}$; and (●) the carbon longitudinal relaxation decay, with a rate $R_C(C_z)$ of 1.79 $s^{-1}$. All intensities are normalized to 100 for the fitted curves at $\tau = 0$. Experimental data are shown together with single-exponential decays $I(\tau) = I_0 \exp(-\tau R)$. (B) Overall rotation correlation time dependence of the six dipolar relaxation rates, calculated using the model free approach. All six rates are satisfied simultaneously by the model free approach when $\tau_n = 6.6$ ns, $S^2 = 0.92$, $\tau_e = 470$ ps, and $\rho_{H^{\alpha}H^i} = 4.1$ $s^{-1}$.

The helical part in the structure of motilin (Figures 5 and 8) is also reflected in the Φ and Ψ values for residues Leu[10]–Lys[16] (Supporting Information, Table 2S). The Φ angles vary between 8 and −100° along this sequence. The angle Ψ is somewat less negative and varies between 5 and −46°, which is a common feature in most helices. The corresponding values for an ideal α-helix are −57° for Φ and −47° for Ψ and for a $3_{10}$-helix are −57° for Φ and −30° for Ψ (Neuhaus & Williamson, 1989). From these values of Φ and Ψ, it is not possible to determine the most likely type of helix.

Table 1: Parameters of the Model Free Spectral Density Function for the $^{13}C^{\alpha}-H^{\alpha}$ Vector in Leu[10] of Motilin in 300 mM SDS, in 30% HFP, and in $D_2O$[a]

| solvent | $\tau_m$ (ns) | $S^2$ | $\tau_e$ (ns) |
|---|---|---|---|
| $D_2O$ | 1.43 | 0.55 | 0.11 |
| 30 % HFP | 3.06 | 0.80 | 0.09 |
| SDS micelles | 6.60 | 0.92 | 0.47 |

[a] Relaxation rates were measured at a 600 MHz proton frequency at 35 °C. The spectral density function was fitted to the mapped spectral densities using a nonlinear Marquardt fitting routine taking into account the relative uncertainties of spectral density values at different frequencies.

*Location of Motilin in the Micelle*. The spin labeling experiments gave the surprising results that 12-doxyl- and 5-doxylstearic acid spin-labels broadened the resonances of the same amino acid residues, Pro[3]-Ile[4]-Phe[5] in motilin, despite the fact that their broadening of the $^{13}C$ resonances of SDS was different. A possible explanation for these results is that there is a specific interaction between the peptide and the spin-label. The peptide concentration in these experiments corresponds to about 1 per 5 micelles. A majority of micelles therefore do not contain a peptide, and these will dominate the $^{13}C$ results for SDS. Although these results show that caution is required in the interpretation of spin-label effects in peptide/micelle complexes, they clearly also show that residues 3−5 of the peptide are located inside the micelle. The experiments with higher 5-doxylstearic acid concentrations showed that only the resonances of a few residues were relatively unaffected. Residues Gln[11], Arg[12], Glu[15], and Lys[16] all belong to one side of the amphiphilic α-helix, as is shown in Figure 8, and we can conclude that they are located on the outer side of the micelle. The results indicate that the hydrophobic N terminal end of motilin is buried inside the SDS micelle and that the helix is located at the micelle surface with one side facing the micelle.

*Dynamics*. The spectral density function corresponding to the so-called model free approach (Lipari & Szabo, 1982a,b) gave a good fit to the determined spectral density values (Figure 9A). A motional model of isotropic rotation could not describe all observed relaxation rates simultaneously (data not shown). Figure 9B shows simulated relaxation rates as a function of the overall rotational correlation time $\tau_m$, using the expressions for the rates given in Peng and Wagner (1992) and the model free spectral density function with the fitted parameters $S^2$ and $\tau_e$ being 0.92 and 0.47 ns, respectively (Table 1). The experimentally measured rates fit all curves well at the fitted $\tau_m$ of 6.6 ns (Figure 9B). This representation of the dynamics illustrates the usefulness of the model free approach in accounting for these experimental results. The contribution to the proton longitudinal relaxation, $\rho_{H^{\alpha}H^i}$, was set to 4.1 $s^{-1}$, as obtained from the spectral density mapping procedure. The correlation time $\tau_m$ used in the structure calculations (5 ns at 28 °C) corresponding to a minimal *R*-factor is in reasonable agreement with the correlation time determined from $^{13}C$ relaxation experiments (6.6 ns at 35 °C). As the full relaxation matrix analysis defines one correlation time

for all residues, it may be estimated to be somewhat faster than that experimentally determined from studies based on the $C^{\alpha}-H^{\alpha}$ spin system of a central residue, due to the flexibility of side chains and the terminal residues.

The high order parameter (0.92, Table 1) indicates that under the conditions used each motilin molecule is associated with a micelle and becomes more rigid in the SDS environment than in $D_2O$. The overall rotational correlation time of motilin in the presence of SDS micelles is approximately 2 times longer compared with the correlation time in the 30% HFP and 4.6 times longer compared with the correlation time in the water environment (Table 1). The overall rotational correlation time of motilin in $D_2O$ fits a model of a sphere consisting of one motilin molecule and a hydration layer of 2.8 Å in $D_2O$ [$\eta = 0.87 \times 10^{-3}$ kg m$^{-1}$ s$^{-1}$, at 35 °C interpolated from the data given in *Spravotchnik Khimika* (1962)]. The corresponding spherical model for a motilin molecule associated with an SDS micelle (60 dodecyl sulfate molecules, one motilin molecule, and a 2.8 Å thick hydration layer) would overestimate the correlation time by 30% compared to the experimentally found value of 6.6 ns. This indicates that somewhat less than 60 dodecyl sulfate molecules may be associated with each motilin molecule.

The present results for motilin indicate an intact complex between the peptide and the micelle at both 35 and 45 °C. As shown in Figure 4, the secondary chemical shifts for the N terminus of motilin in SDS are not particularly temperature-dependent, which suggests that a rigidly structured N terminus exists also at the higher temperature.

The overall rotational correlation times of 6.6 and 4.5 ns at 35 and 45 °C, respectively, determined here for motilin can be compared to other reported correlation times for peptides bound to SDS micelles. Henry et al. (1986) have reported a $\tau_m$ of 11 ns for a dimer of the 50-residue bacteriophage M13 coat protein dissolved in SDS at 23 °C, as measured by $^{13}C$ NMR relaxation studies of the methyl groups of 3-$^{13}C$-labeled alanines. Orekhov et al. (1994) have reported a correlation time of 6.6 ns for (1−71) bacterioopsin in 300 mM SDS at 50 °C by heteronuclear $^{1}H-^{15}N$ relaxation experiments. Spyracopoulos et al. (1996) have studied the 20-residue peptide alamethicin in SDS micelles by heteronuclear $^{1}H-^{15}N$ relaxation experiments. They found a $\tau_m$ of 5.7 ns in 150 mM SDS at 27 °C. The correlation times reported in these studies were all interpreted via Stokes' law, and assuming 60 SDS molecules per micelle, except in the alamethicin study, where the micelles were estimated to contain about 40 SDS molecules. A more recent study of the dynamics of the bacteriophage M13 coat protein in a 500 mM SDS solution at 37 °C has been published (Papavoine et al., 1997). They studied $^{15}N$ relaxation and found an overall correlation time of 11.8 ns.

In order to investigate the general properties of SDS micelles as a solvent system for peptides/proteins, we performed a closer comparison of these results and ours on motilin. In this comparison, we assumed that the complexes have a spherical shape. Taking into account the solvent viscosity of either $D_2O$ or $H_2O$, we could use Stokes' law to calculate an effective volume of the sphere from the reported values of $\tau_m$ (Figure 10). Temperature-dependent viscosity values were used for $H_2O$ (*CRC Handbook of Chemistry and Physics*, 1968) and $D_2O$ (*Spravotchnik Khimika*, 1962). The theoretical curves for the volumes of peptide-containing micelles as a function of the molecular mass of the peptide

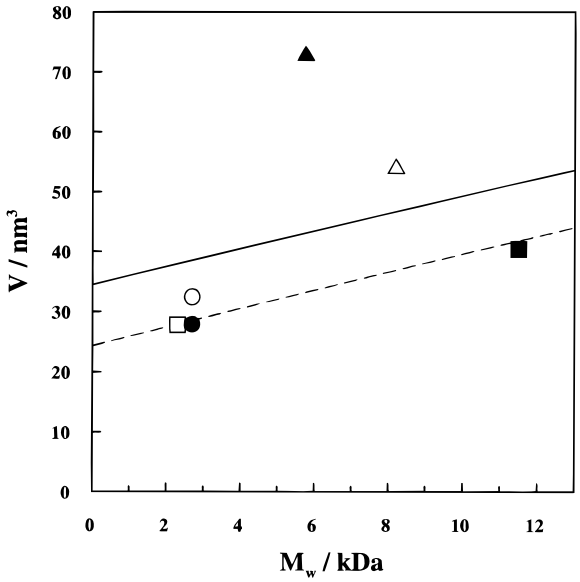


FIGURE 10: Volumes corresponding to reported rotational correlation times of SDS micelles containing different peptides as a function of peptide molecular weight. The volumes were calculated using Stokes' law, $\tau_m = \eta V(kT)^{-1}$, where $\eta$ is the viscosity of the solvent, $V$ is an effective volume, $k$ is the Boltzmann constant, and $T$ is the absolute temperature. Temperature-dependent viscosity values for $H_2O$ (*CRC Handbook of Chemistry and Physics*, 1968) and $D_2O$ (*Spravotchnik Khimika*, 1962) were used. The symbols represent (○) motilin at 35 °C (present study), (●) motilin at 45 °C (present study), (□) alamethicin at 27 °C (Spyracopoulos et al., 1996), (■) the M13 dimer at 23 °C (Henry et al., 1986), (△) bacterioopsin at 50 °C (Orekhov et al., 1994), and (▲) the M13 monomer at 37 °C (Papavoine et al., 1997). The solid and dashed lines represent curves corresponding to the volume of a micelle consisting of 60 or 40 SDS molecules, respectively, with one peptide and a 2.5 Å thick hydration layer. The curves were calculated as $V = V_{SDS} + V_{peptide} + V_{hydration}$. The volume of SDS, $V_{SDS}$, was obtained by multiplying the volume of a dodecyl sulfate molecule, 0.35 nm$^3$ (Israelachvili, 1991), by the number of dodecyl sulfates forming one peptide-containing micelle (60 or 40). The volume of the peptide was calculated using the specific volume of proteins and peptides, 0.73 g/cm$^3$ (Cavanagh et al., 1996), and the molecular mass of the peptide.

are also included in Figure 10, assuming 60 or 40 dodecyl sulfate molecules and one peptide per micelle with a 2.5 Å hydration layer. The combined results of these studies, as presented in Figure 10, are all compatible with a model where the proteins or peptides are encompassed in micelle-like structures with a size similar to that of the free micelle. The largest deviation from the model and the largest volume was found for the M13 protein in 500 mM SDS (Papavoine et al., 1997) and may possibly be explained by the high SDS concentration and a correspondingly increased micelle size. Another contributing factor could be a higher viscosity at high SDS concentrations (Chari et al., 1993), which would lead to an overestimated volume by our calculations.

*Concluding Remarks*. In the present study, we have presented a detailed description of the structure, dynamics, and location of a peptide hormone associated with a micelle. The association of motilin with the SDS micelle apparently constrains the flexibility of the motilin solution structure. This relatively well-ordered structure, which should mimic a membrane-associated peptide, can be determined by NMR with good precision. The membrane-associated structure and location relative to the membrane surface should be significant for recognition by the membrane-bound hormone receptor.

## ACKNOWLEDGMENT

We thank the Swedish NMR Center for use of the VARIAN UNITY 600 MHz spectrometer. The Swedish NMR Center staff Toshi Nishida, Charlotta Damberg, and Lotta Johansson are acknowledged for skillful help. We thank Dr. A. Ehrenberg for stimulating discussions and Dr. P. Allard for valuable suggestions at the initial stage of experiments related to the spectral density mapping. Mr. Torbjörn Astlind is acknowledged for skilled computer assistance and for help in the setup of deuterium decoupling experiments. We thank Ms. Britt-Marie Olsson for peptide synthesis and for the HPLC purification.

## SUPPORTING INFORMATION AVAILABLE

Tables 1S−3S with chemical shift assignments, $^3J_{H^\alpha H^N}$ coupling constants and corresponding Φ torsion angles, and torsion angles calculated from the lowest-energy conformation of motilin in 300 mM SDS micelles at 28 °C and graph (Figure 1S) showing the total energy and NOE constraint energies for the 120 calculated structures of motilin (4 pages). Ordering information is given on any current masthead page.

## REFERENCES

Allard, P., Jarvet, J., Ehrenberg, A., & Gräslund, A. (1995) *J. Biomol. NMR 5*, 133−146.

Arvidsson, K., Jarvet, J., Allard, P., & Ehrenberg, A. (1994) *J. Biomol. NMR 4*, 653−672.

Baleja, J., Moult, J., & Sykes, B. (1990) *J. Magn. Reson. 87*, 375−384.

Bax, A., & Davis, D. G. (1985) *J. Magn. Reson. 65*, 355−366.

Borgias, B. A., & James, T. L. (1990) *J. Magn. Reson. 87*, 475−487.

Boulanger, Y., Khiat, A., Chen, Y., Gagnon, D., Poitras, P., & St-Pierre, S. (1995) *Int. J. Pept. Protein Res. 46*, 527−534.

Brown, J. C., Cook, M. A., & Dryburgh, J. R. (1973) *Can. J. Biochem. 51*, 533−537.

Brown, L., Braun, W., Kumar, A., & Wüthrich, K. (1982) *Biophys. J. 37*, 319−328.

Brünger, A. T. (1992) *X-PLOR Manual*, version 3.0.

Cavanagh, J., Fairbrother, W. J., Palmer, A. G., III, & Skelton, N. J. (1996) *Protein NMR Spectroscopy: Principles and Practice*, p 18, Academic Press Inc., San Diego.

Chari, K., Antalek, B., Lin, M. Y., & Sinha, S. K. (1993) *J. Chem. Phys. 100*, 5294−5300.

Chupin, V., Killian, A., Breg, J., de Jongh, H., Boelens, R., Kaptein, R., & de Kruijff, B. (1995) *Biochemistry 34*, 11617−11624.

Cooke, R., Carter, G., Murray-Rust, P., Hartshorn, M., Herzyk, P., & Hubbard, R. (1992) *Protein Eng. 5*, 473−477.

*CRC Handbook of Chemistry and Physics* (1968) 49th ed., CRC Press, Cleveland, OH.

Creighton, T. E. (1993) *Proteins*, p 225, W. H. Freeman and Co., New York.

Dayie, K. T., & Wagner, G. (1994) *J. Magn. Reson. A 111*, 121−126.

Depoortere, I., Peeters, T. L., & Vantrappen, G. (1990a) *Gastroenterology 98*, A489.

Depoortere, I., Peeters, T. L., & Vantrappen, G. (1990b) *Peptides 11*, 515−519.

Depoortere, I., Peeters, T. L., & Vantrappen, G. (1993) *J. Recept. Res. 13*, 903−923.

Edmondson, S., Khan, N., Shriver, J., Zdunek, J., & Gräslund, A. (1991) *Biochemistry 30*, 11271−11279.

Griesinger, C., Otting, G., Wüthrich, K., & Ernst, R. R. (1988) *J. Am. Chem. Soc. 110*, 7870−7872.

Henry, G., Weiner, J., & Sykes, B. (1986) *Biochemistry 25*, 590−598.

Israelachvili, J. (1991) *Intermolecular and Surface Forces*, pp 366−374, Academic Press, San Diego.

Jarvet, J., Allard, P., Ehrenberg, A., & Gräslund, A. (1996) *J. Magn. Reson. B 111*, 23−30.

Jeener, J., Meier, B. H., Bachman, P., & Ernst, R. R. (1979) *J. Chem. Phys. 71*, 4546−4553.

Kemmink, J., & Creighton, T. E. (1995) *Biochemistry 34*, 12630−12635.

Khan, N., Gräslund, A., Ehrenberg, A., & Shriver, J. (1990) *Biochemistry 29*, 5743−5751.

Koga, H., Sato, T., Tsuzuki, K., Onoda, H., Kuboniwa, H., & Takanashi, H. (1994) *Bioorg. Med. Chem. Lett. 4*, 1347−1352.

Koradi, R., Billeter, M., & Wüthrich, K. (1996) *J. Mol. Graphics 14*, 51−55.

Kumar, A., Wagner, G., Ernst, R. R., & Wüthrich, K. (1981) *J. Am. Chem. Soc. 103*, 3654−3658.

Levitt, M. H., Freeman, R., & Frenkiel, T. (1982) *J. Magn. Reson. 47*, 328−330.

Lipari, G., & Szabo, A. (1982a) *J. Am. Chem. Soc. 104*, 4546−4559.

Lipari, G., & Szabo, A. (1982b) *J. Am. Chem. Soc. 104*, 4559−4570.

Macielag, M. J., Peeters, T. L., Koneatis, Z. D., Florance, J. R., Depoortere, I., Lessor, R. A., Bare, L. A., Cheng, Y., & Galdes, A. (1992) *Peptides 13*, 565−569.

Macielag, M. J., Marvin, M. S., Peeters, T. L., Dharanipragada, R., Depoortere, I., Florance, J. R., Lessor, R. A., & Galdes, A. (1994) in *Peptides Chemistry, Structure and Biology* (Hodges, R. S., & Smith, J. A., Eds.) pp 681−683, Escom, Leiden.

McDonnell, P. A., & Opella, S. J. (1993) *J. Magn. Reson. B 102*, 120−125.

McIntosh, C. H. S., & Brown, J. C. (1988) in *Advances in Metabolic Disorders* (Luft, R., Levine, R., & Mutt, V., Eds.) Vol. 11, pp 439−455, Academic Press, New York.

Miller, P., Gagnon, D., Dickner, M., Aubin, P., St-Pierre, S., & Poitras, P. (1995) *Peptides 16*, 11−18.

Mutt, V. (1982) *Vitam. Horm. (N.Y.) 39*, 231.

Neuhaus, D., & Williamson, M. P. (1989) *The Nuclear Overhauser Effect in Structural and Conformational Analysis*, Figure 6.18, Table 6.2, p 226, VCH Publishers Inc., New York.

Nikonowicz, E., Meadows, E., & Gorenstein, D. (1990) *Biochemistry 29*, 4193−4204.

Nilges, M., Gronenborn, A. M., Brünger, A. T., & Clore, G. M. (1988) *Protein Eng. 2*, 27−38.

Orekhov, V., Pervushin, K., & Arseniev, A. (1994) *Eur. J. Biochem. 219*, 887−896.

Papavoine, C., Konings, R., Hilbers, C., & van de Ven, F. (1994) *Biochemistry 33*, 12990−12997.

Papavoine, C., Remerowski, L., Horstink, L., Konings, R., Hilbers, C., & van de Ven, F. (1997) *Biochemistry 36*, 4015−4026.

Pastore, A., & Saudek, V. (1990) *J. Magn. Reson. 90*, 165−176.

Peters, T. L., Matthijs, G., Depoortere, I., Cachet, T., Hoogmartens, J., & Vantrappen, G. (1989) *Am. J. Physiol. 257*, G470−G474.

Peeters, T. L., Macielag, M. J., Depoortere, I., Konteatis, Z. D., Florance, J. R., Lessor, R. A., & Galdes, A. (1992) *Peptides 13*, 1103−1107.

Peng, J. W., & Wagner, G. (1992) *J. Magn. Reson. 98*, 308−332.

Poitras, P. (1994) in *Gut Peptides, Motilin* (Walsh, J. H., & Dockray, G. J., Eds.) pp 261−304, Raven Press Ltd., New York.

Poitras, P., Gagnon, D., & St-Pierre, S. (1992) *Biochem. Biophys. Res. Commun. 183*, 36−40.

Poitras, P., Miller, P., Dickner, M., Mao, Y. K., Daniel, E. E., St-Pierre, S., & Trudel, L. (1996) *Peptides 17*, 701−707.

Richardson, J. (1981) *Adv. Protein Chem. 34*, 167−339.

Schubert, H., & Brown, J. C. (1974) *Can. J. Biochem. 52*, 7−8.

Sönnichsen, F. D., Van Eyk, J. E., Hodges, R. S., & Sykes, B. D. (1992) *Biochemistry 31*, 8790−8798.

*Spravotchnik Khimika* (1962) 2nd ed., Vol. 1, pp 985−987, Moskva.

Spyracopoulos, L., Yee, A., & O'Neil, J. (1996) *J. Biomol. NMR 7*, 283−294.

States, D. J., Haberkorn, R. A., & Ruben, D. J. (1982) *J. Magn. Reson. 48*, 286−292.

Sutcliffe, M. J. (1993) in *NMR of Macromolecules a Practical Approach* (Roberts, C. C. K., Ed.) p 362, Oxford University Press, Oxford.

Wüthrich, K. (1986) *NMR of Proteins and Nucleic Acids*, p 17, Wiley, New York.

BI970193B